Selection of diffractively produced $\eta\pi$ and $\eta'\pi$ final states at the COMPASS experiment

Rocio Reyes Ramos

Masterarbeit in Physik
angefertigt Helmholtz-Institut für Strahlen- und Kernphysik

vorgelegt der
Mathematisch-Naturwissenschaftlichen Fakultät
der
Rheinischen Friedrich-Wilhelms-Universität
Bonn

Mai 2018

I hereby declare that this thesis was formulated by myself and that no sources or tools other than those cited were used.

Bonn, ...
Date Signature

1. Gutachter: Prof. Dr. Bernhard Ketzer
2. Gutachterin: Jun. Prof. Dr. Annika Thiel

Acknowledgements

I want to give many thanks to my advisor Prof. Dr. Bernhard Ketzer, first for answering that first email that opened the door for me to come to Germany and work in his group, and second, for everything else that happened next. The work I have been doing here, provided me such a valuable experience in coding, analysis and detector physics. Being an expert on-call for the GEM detectors allowed me to travel to CERN and to become a member of the COMPASS collaboration. Thank you for this opportunity.

Also I want to thank Jun. Prof. Annika Thiel for being my second referee and for taking time to attend my master colloquium.

Many thanks to the COMPASS collaboration for the chance to work together on various projects. Thanks to the people that I met during my shifts and at the workshops, for their advice and help, thank you to the colleagues at Munich for answering my questions via email.

Obviously I would not be here without the help of my incredible family, my parents Juan Antonio and Pati, and my sister Erandi. Thank you for your sacrifices, love and financial support. Muchas, muchas gracias por todo, los quiero.

Thank you to my family in San Luis Potosí, Salinas, Matehuala, Metepec, Ciudad de México, Guanajuato, Morelia and Hawaii who did not forget about me, and kept worrying and sending me good vibes and love.

To Aaron, being my uncle on this side of the world, thank you for taking care of me.

To my long time friends that on difficult times lend me an ear to help me, especially to Ericka that was always there to bring me back to earth. To both Césars and Ramsés, who welcomed me and offered their support and solidarity.

To the little México I found in this country that allowed me to keep talking with mexican slang, and eating traditional food (with the weirdest ingredients) and of course drinking tequila.

To my office mates, Liza and Mathias. Thank you for all the laughs, for sharing with me the expert on-call job, thank you for the incredible help during the realization of this thesis, which included correcting codes and doing the spell check of my text in a short time and for killing bugs in the office during the night shifts.

The biggest thanks goes to Misha, who was there also from the very beginning. He always has a storm of ideas about how to approach a physics problem; he is a very active person and shares that energy with all the people around him. Thank you for teaching me patiently, thank you for the riddles and hiking trips, thank you for all your help during my studies.

Contents

CHAPTER 1

Introduction

The COMPASS[1] experiment at CERN[2] uses a π^- beam with an energy of 190 GeV scattering off a liquid hydrogen target to study the excitation spectrum of light isovector mesons. Of special interest are intermediate states with exotic quantum numbers, which are predicted by Quantum Chromo Dynamics (QCD) but are difficult to find because they cannot be formed by a simple $q\bar{q}'$ system. Some of these quantum numbers can be directly accessed via diffractive $\eta^{(\prime)}\pi^-$ production at COMPASS (Figure 1.1).

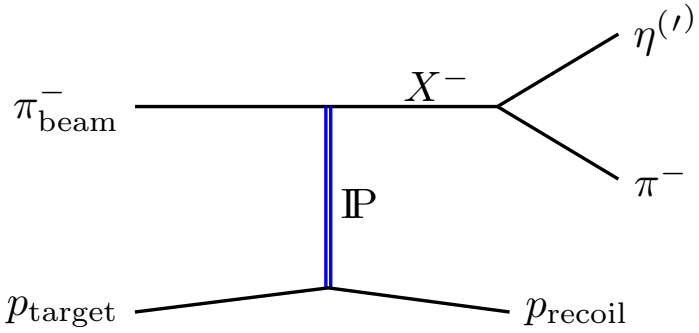

Figure 1.1: The $\eta\pi$ and $\eta'\pi$ production diagramm

A first analysis of these states has been published [1]. Compared to this, we make use of an improved reconstruction of charged particles and especially an improved photon reconstruction in the calorimeters, which is expected to increase the data set. The event selection on this data set, is the main goal of this master thesis.

In the first chapter it is discussed in more detail why these final states are particularly interesting.

Afterwards the COMPASS experiment is introduced, as well as its design and the analysis software that was used for the event selection.

The main part covers the details of the event selection and explains the steps needed to arrive at a clean sample of $\eta^{(\prime)}\pi^-$ events. The next chapter talks about how the event selection was performed.

[1] COmmon Muon Proton Apparatus for Structure and Spectroscopy
[2] Conseil Européen pour la Recherche Nucléaire

The final part shows the resulting invariant mass spectra of the $\pi^+\pi^-\pi^0$ system and the $\eta^{(\prime)}\pi^-$ system where one already can identify some of the peaks as particles. Finally we can also compare the results to the previous analysis.

CHAPTER 2

Theory

Before starting, it is important to mention that this thesis is using natural units notation, $\hbar = c = 1$; the units for masses, momenta and energies are eV, velocities are dimensionless, and times and distances corresponds to eV^{-1}.

2.1 Exotic quantum numbers

Hadrons are divided in two groups: states with integer spin are called mesons, and the states with half integer spin are called baryons. The constituent quark model suggests a picture of baryons as a composite object which contains three quarks, and mesons being made up of a quark and an antiquark. Mesons that are formed by the quarks *up* (u), *down* (d) or *strange* (s), are called light mesons.

In the constituent quark model the quantum numbers of meson can be understood as follows.

The u and d quarks form an isospin doublet, I= 1/2 , $\mathrm{I}_3 = \pm 1/2$. With combining those numbers for the $q\bar{q}'$ system, the possible states are:

$$\text{isoscalar I} = 0 \text{ or isovector I} = 1$$

Quarks have spin 1/2, which yields a total intrinsic spin for the mesons of

$$S = 0 \text{ or } S = 1$$

The total angular momentum J is formed by the spin and the orbital angular momentum. It lies in the range:

$$|L - S| \leq J \leq L + S.$$

For the parity P, fermions and anti fermions have opposite intrinsic parity, that gives for the meson:

$$P = (+1)(-1)(-1)^L = (-1)^{L+1}$$

The C-parity is only well defined for neutral mesons, that consist of a quark q and its corresponding antiquark $\bar{q}$:

$$C = (-1)^{L+S}$$

For charged mesons C-parity is not defined. However, by an additional rotation of 180° around the I_2 axis in the isospin space, which corresponds to a charge flip, charged mesons, containing

u and d quarks/antiquarks become eigenstates of the G-parity with eigenvalue

$$G = (-1)^{L+S+I}$$

The notation that is used to describe the quantum numbers of a mesons is:

$$I^G J^{PC}$$

An example of the possible quantum numbers that can be obtained are listed in Table 2.1.

L	S	J^{PC}	Particles
0	0	0^{-+}	π, $\eta^{(\prime)}$
	1	1^{--}	ρ, ω
1	0	1^{+-}	b_1, h_1
	1	0^{++}	a_0, f_0
		1^{++}	a_1, f_1
		2^{++}	a_2, f_2

Table 2.1: Possible quantum numbers for a $q\bar{q}'$ system. The first particle name corresponds to the isovector and the second is the isoscalar.

However, there are some numbers that cannot be produced using these rules. Those are called spin-exotic quantum numbers:

$$J^{PC} = 0^{--}, 0^{+-}, 1^{-+}, 2^{+-}, ...$$

2.2 Channels $\eta\pi$ and $\eta'\pi$

These channels allow to search such exotic states.

For example, $\eta^{(\prime)}$ and $\pi^{\pm}$ have the quantum numbers:

$$J^{PC} = 0^{-+}$$

so for the system $X \to \eta^{(\prime)}\pi^-$, the numbers that are obtained are:

$$C(X) = C(\eta^{(\prime)}) \cdot C(\pi) = +$$

$$P(X) = P(\eta^{(\prime)}) \cdot P(\pi) \cdot (-1)^L = (-1)^L$$

Since both $\eta^{(\prime)}$ and π^- do not have intrinsic spin the total spin J of the $\eta^{(\prime)}\pi^-$ system is equal to the orbital angular momentum L.

$$J^{PC} = L^{(-1)^L +}$$

Giving us the possible quantum numbers: $J^{PC} = 0^{++}, 1^{-+}, 2^{++}, 3^{-+}, ...$, where the combinations with odd spin J: 1^{-+} and $3^{-+}, ...$ are exotic.

To study those systems, diffractive scattering of a π beam off a fixed proton target can be used.

In this reaction the proton remains intact and the beam particle is excited to the intermediate state X, which immediately shows us that:

$$I^G(X) = I^G(\pi) = 1^-$$

Afterwards X decay into the desired final state $\eta^{(\prime)}\pi^-$.
The sought reaction is:

$$\pi^- + p \to X^- + p \to \eta^{(\prime)}\pi^- + p$$

Then it is important to discuss the decay channels of the $\eta^{(\prime)}$ to the final states where it can be observed using the COMPASS setup.

Have a look at the decay channels of the reaction for the final outgoing particles. For η (m_η =547.8 MeV and Γ_η =1.3 keV), the prominent decays are [2]:

- $\to \gamma\gamma$; BR[1]: 39.4 %
- $\to 3\pi^0$; BR: 32.5 %
- $\to \pi^+\pi^-\pi^0$; BR: 22.9 %

For the η' ($m_{\eta'}$ =957.7 MeV and $\Gamma_{\eta'}$ =0.199 MeV), the prominent decays are [2]:

- $\to \pi^+\pi^-\eta$; BR: 42.9 %
- $\to \rho^0\gamma$; BR: 29.1 %
- $\to \pi^0\pi^0\eta$; BR: 22.3 %

The π^0, whose mass is m_{π^0} =134.9 MeV, dominantly decays to $\to \gamma\gamma$ with a BR of 98.8 %.

The decays for $\eta \to 3\pi^0$, $\eta' \to \pi^0\pi^0\eta$ are not investigated, due to the fact that at the final stage there are six γ, and that many photons are difficult to reconstruct and separate in the electromagnetic calorimeter (ECAL), due to the combinatorial background.

The channel $\eta\pi^- \to \gamma\gamma\pi^-$ is also not studied, because with only one charged particle, the reconstruction of the interaction point is troublesome. However the decay $\eta \to \gamma\gamma$ is used for the $\eta' \to \pi^+\pi^-\eta$, in order to have the same final state consisting out of three charged π and two photons.

The chosen reaction I am focusing, is depicted in the diffractive diagramm in Figure 2.1. Where the Pomeron ($\mathbb{P}$) is the exchange particle for this process and can be pictured as a multi-gluon state.

This type of reactions can be produced by the COMPASS experiment, that will be described in the next chapter 3.

[1] branching ratio

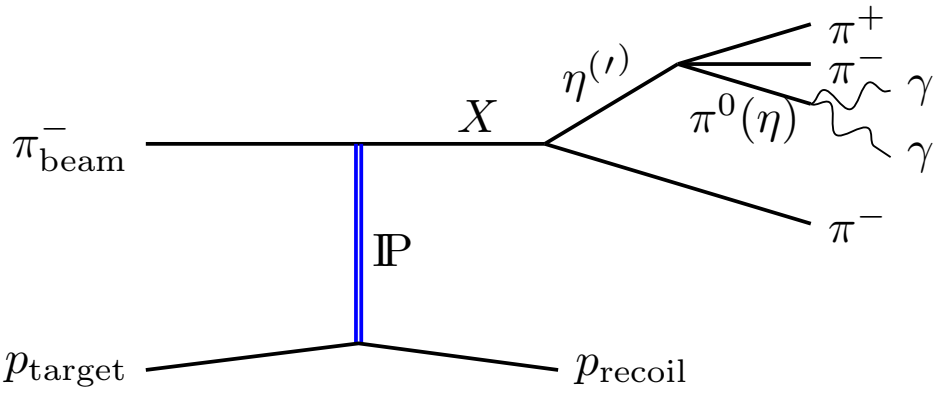

Figure 2.1: The $\eta\pi$ and $\eta'\pi$ production diagramm.

CHAPTER 3

COMPASS experiment

The following description of the setup and general information about the spectrometer was collected from the COMPASS articles: [3] and [4].

The **CO**mmon **M**uon **P**roton **A**pparatus for **S**tructure and **S**pectroscopy (**COMPASS**) is a fixed target experiment located at the M2 beamline of the Super Proton Synchrotron (SPS) in the north area of the **C**onseil **E**uropéen pour la **R**echerche **N**ucléaire (**CERN**).

COMPASS itself is a 60 m long, two-staged magnetic spectrometer, which uses the high intensity proton beam from the SPS and converts it to muon or hadron beams 3.1.1. Each of the spectrometers has magnets, particle identification, calorimetry and tracking detectors. The goal of the experiment is to have a better understanding of the structure and dynamics of hadrons. This thesis will focus on the setup used in the year 2008 where a 190 GeV beam of negatively charged hadrons and a liquid hydrogen target were used.

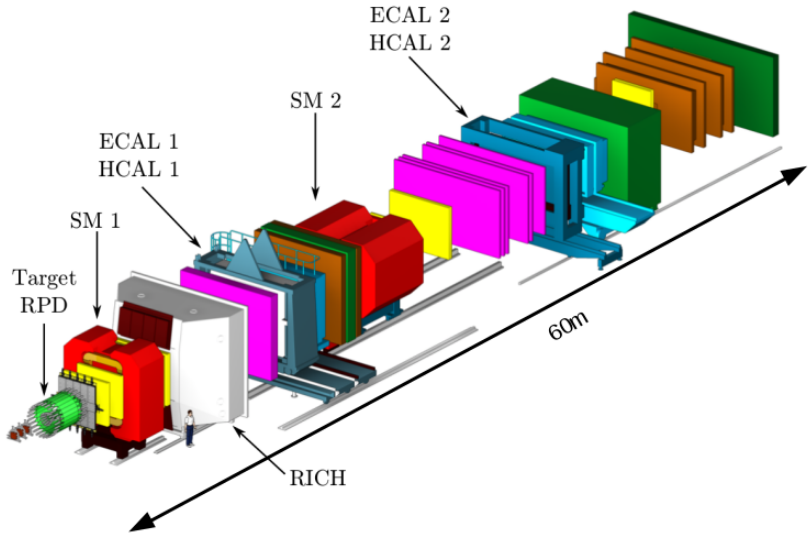

Figure 3.1: Design of COMPASS experiment for hadron beam (from [3], modified)

3.1 Design of the experiment

3.1.1 Beam

The negative hadron beam with an energy of 190 GeV was obtained after the following steps. First 400 GeV protons are extracted from the SPS onto a primary beryllium target of 80 mm wide, 3 mm high and 500 mm thick. The average beam intensity is $5 \times 10^6\,\mathrm{s}^{-1}$. Next, the beam goes through a line of 1.1 km that has optical equipment for focusing and defocusing, and dipole magnets to select the moment of the beam. Before the hadron beam interacts with the target at COMPASS there are two Cherenkov counters (CEDARs), that identify the beam particles.

The result is a negative hadron beam, with a relative composition of:

Beam momentum	Particle	Percentage
190 GeV	π^-	96.8 %
	K^-	2.4 %
	$\bar{p}$	0.8 %

3.1.2 Target

The π^- beam interacts with the liquid hydrogen target at COMPASS. It has a cylindrical shape of 40 cm long with a diameter of 35 mm. The diameter of the target is matched to the dimensions of the beam spot ($\sigma \approx$8 mm).

Surrounding the target there are two segmented concentric cylindrical barrels of plastic scintillators, which form the Recoil Proton Detector (RPD).

The inner ring is segmented in 12 slabs of scintillators positioned at a radius of 12 cm. The outer ring is segmented in 24 slabs of plastic scintillators, with a radius of 75 cm. Each element covers an azimuthal angle of 15°. In order to optimise the azimuthal angle resolution, the outer ring is positioned such that each inner ring counter faces three outer ring slabs as despicted in Figure **??**

This detector measures the recoiling protons, which ensure the exclusivity of the final state, and is also used as a trigger.

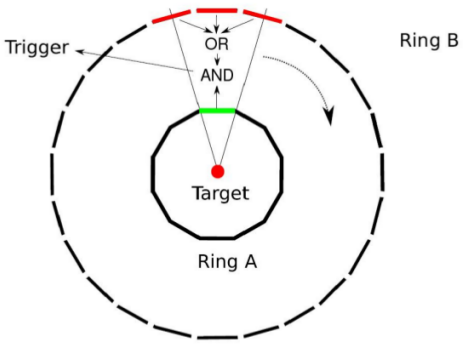

Figure 3.2: Recoil proton detector [3]

3.1.3 Trigger

The trigger system is considered as the first stage of the Event Selection, because the detectors that are part of it will reject the events that are not of further interest. Their purpose is to reduce the dead time of the data acquisition (DAQ).

One of the main trigger systems is the Diffractive Trigger (DT0) that is formed by the signals of the following detectors (also see Figure 3.3):

- alternative Beam trigger (aBT): It is a coincidence of the signal from the X-plane of the SciFi 1 (Scintillating Fibre Counter) with the signal from the Beam Counter (BC). This trigger selects incoming beam particles and defines the reference time of the event. They are both localized upstream of the target region.
- Recoil Proton Detector (RPD): this detector is located at the target area (3.1.2) and selects events with recoiling protons from the target.
- No veto ($\overline{VETO}$): it helps to select only the events of interest, and is formed by the signals from:
  - Beam killers: there are two scintillating counters, if a signal is obtained from them, it would mean that the beam did not interact with the target, therefore this event will be rejected.
  - Sandwich veto detector: it is used to veto the charged and neutral particles that are detected outside of the angular acceptance of the spectrometer and the RPD.
  - Hodoscope veto system: removes events with a large deviation from the nominal beam position and direction.

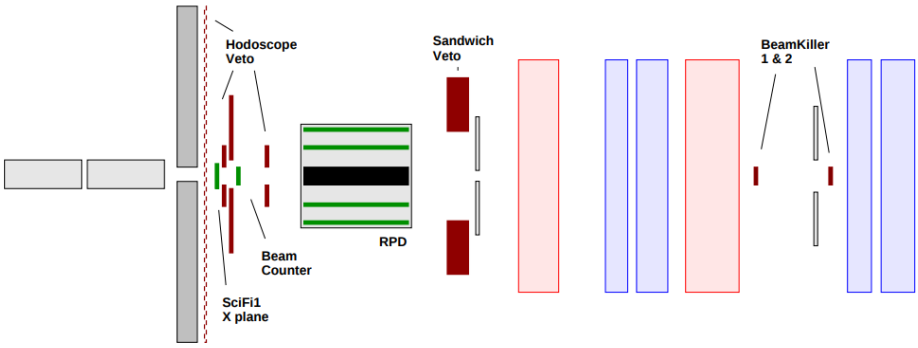

Figure 3.3: DT0 trigger elements in COMPASS [5]. (schematic view, not to scale)

3.1.4 LAS and SAS

The Large Angle Spectrometer (LAS) includes all detectors around SM1, so everything between target and SM2. Measure scattered particles with polar angles $-180\,\text{mrad} \leq \theta \leq 180\,\text{mrad}$. The Ring Imaging Cherenkov detector (RICH) can identify particles with a momentum less than

43 GeV. The Small Angle Spectrometer (SAS) is formed by the detectors located downstream of the SM1 magnet. It detects particles at small angles 30 mrad and large momenta of 5 GeV and higher.

3.1.5 Electromagnetic Calorimeters (ECALs)

These detectors register photons, which get absorbed and produce scintillation light, which can be detected by photomultipliers. ECAL1 is located at LAS, it is formed by three types of lead glass blocks, 1500 blocks in total, each read out by a photomultiplier tube. ECAL2 located at SAS, consists of 3068 lead-glass blocks.

Reconstruction on ECALs

Event reconstruction in ECAL1 and ECAL2 is performed by using time and signal amplitude information. The signal amplitude for each module is converted into energy applying conversion coefficients that were derived from the calibration with an electron beam. The variation of the amplitudes over the data taking period is accounted for by using the information provided by the Laser and LED monitoring sys- tems. The energy calibration of each module is further improved by using the data derived from an analysis of the $\pi^0 \to \gamma\gamma$ decay process. For both ECALs, the event reconstruction consists of associating an energy deposit in one or several adjacent modules to a single incident particle. A set of energy deposits that is assumed to originate from a single particle is called in the following a shower; the full energy deposit and hit position of the particle are calculated from it. In many cases, two or more showers overlap and form a cluster.

This means to connect adjacent digits, that are supposed to result from the same particle trajectory, into one common object.

3.2 Analysis tools for COMPASS data

The raw data obtained from the detectors, has to be reconstructed and analyzed, for this purpose the tool CORAL and the framework PHAST are used, both softwares are based on ROOT.

COMPASS **R**econstruction and **A**na**L**ysis project (CORAL) processes the raw data files and obtains values from the detectors, like timing, signal amplitudes or hits and with this information it is able to reconstruct the tracks, vertices, clusters and more for each event. The files obtained at the end are called **m**ini **D**ata **S**ummary **T**rees (mDST).

The next step is to acces this mDST files and analyzed them. This is done using the framework **PH**ysics **A**nalysis **S**oftware **T**ool (PHAST). This one contains classes that are called by user-defined functions specified in C++ programs called UserEvent(number).cc. With these functions the data can be filtered for every event of the mDST, allowing to make an Event Selection. The output can be two types of files. The first one is a microDST that is full of events and can be processed with PHAST once more, and the second type of file is a ROOT file.

ROOT is an interactive tool, written in C++ and developed at CERN, that allows the analysis, visualization and presentation of data from high-energy physics.

To access huge amount of data, ROOT provides a data structure *tree* on an event-by-event basis. With its different packages it allows to create histograms, do fittings.

3.2.1 Reconstruction of events

Track reconstruction

In order to reconstruct trajectories of charged particles one has to find candidate hits that can be connected by a trajectory that goes through the detectors. As a last step of the track reconstruction, the track fitting is done by application of the full Kalman filter, where all the candidates are added to the fit.

3.2.2 Vertex reconstruction

The interaction point, called vertex, needs to be identified. To perform the vertex reconstruction, charged tracks reconstructed in the spectrometer and in the beam telescope are used. Only tracks with momentum can be used for this procedure. From these tracks the initial interaction point can be defined by averaging the z coordinate of the points closest to the beam track. Then the inverse Kalman filter is applied to remove the outliers.

CHAPTER 4

Event Selection

The complete Slot 4 production of the 2008 hadron data with negative beam is divided in three periods of data taking: W33, W35, and W37, in total they contain 7.4×10^9 events [6].

4.1 First stage of selection

4.1.1 Diffractive Trigger (DT0)

DT0 is one of the main triggers at COMPASS, and it is used during data taking. It is formed by the signals aBT && RPD && $\overline{VETO}$ (see section 3.1.3 for details).

In Figure 4.1 the blue histogram represents the events that were selected by this trigger. The column for the RPD in Figure 4.1 shows the number of events for only this trigger, during data taking it was not saved. However, the RPD signal is a requirement of DT0 and therefore is present in the final data.

Despite the DT0 is formed by a $\overline{VETO}$ signal, e.g. the column for the Inner Veto (VI) still has some events. The reason is in the way the signals for the vetos are combined. The total trigger veto *VETO* is constructed as a coincidence of the signals from all the vetos of the experiment. On the other hand, the VI trigger is formed by only Veto_Inner1 and Veto_Inner2 with a wider gate for the coincidence. For example, if two events are happening in a very short time range, the first event might trigger the vetos which results in a "true" for *VETO* and VI. If now the next event did not activate the vetos, *VETO* is false, but VI might still be true because of the wide coincidence gate [7]. However, this is a small effect as we can also see in the histogram.

4.2 Preselection events

An event preselection was done by Stephan Wallner, with the intention of reducing the amount of data [8]. The following cuts were applied:

- The event must have a best primary vertex **??**
- The primary vertex must lie within the interval: $-200\,\mathrm{cm} < z_{\mathrm{PV}} < 160\,\mathrm{cm}$
- The number of tracks leaving the primary vertex is 1 or 3
- The sum of the charges of all three tracks must be equal to -1

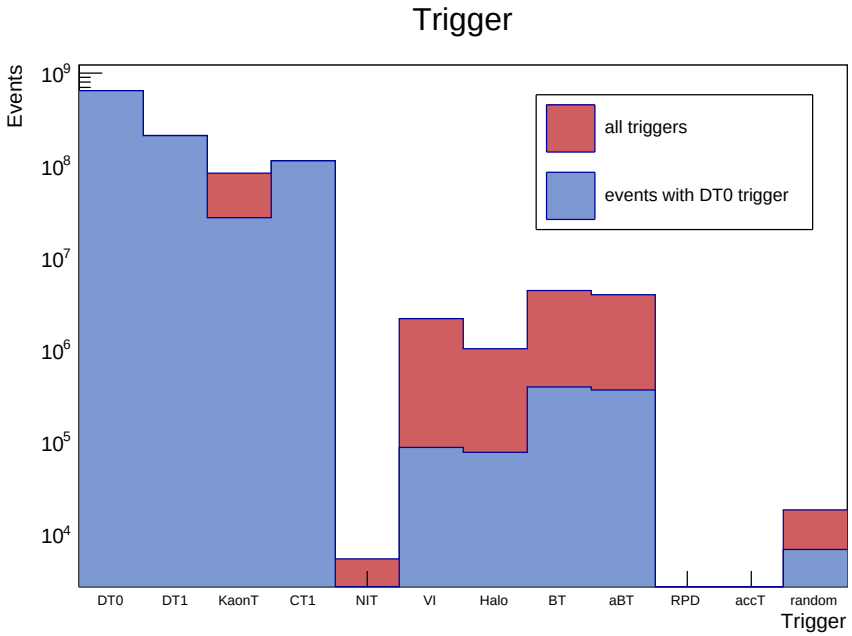

Figure 4.1: All the triggers for the negative hadron beam used in the 2008 data taking. In red are all the events of each trigger and in blue are the events selected by the DT0 trigger.

The final mDST, with 7.1×10^8 events, and 3 TB were copied from the tapes at CERN. The event selection stage for this work was performed using the CB-HISKP[1] cluster. The data reduction program was executed in parallel on 100 nodes using the HT-CONDOR job distribution system.

4.2.1 Best primary vertex and its position

The strong interaction has a lifetime of the order of 10×10^{-22} s, which means the particles produced in the reaction will decay immediately, therefore, for the diffractive system it is important to get the interaction point of the beam with the target.

The point of interaction, in other words the primary vertex, is defined in CORAL by the crossing of one reconstructed beam track with tracks of the outgoing particles [9]. For this a vertex fit method is applied. This method can give us various primary vertices and for this reason we define a best primary vertex, as the vertex with the least χ^2.

To ensure the best primary vertex is in the target area, its position (x, y, z) is required to be (Figures 4.2,4.3):

- $-75\,\text{cm} < z < 25\,\text{cm}$
- $r = \sqrt{x^2 + y^2} < 2\,\text{cm}$

There are more structures seen in the $\mathrm{d}N/\mathrm{d}z$ distribution, for example in Figure 4.2 at -20 cm and -15 cm the two insulating windows of the target are visible. In Figure 4.3 one can see two circles, that are the boarders of the target container and the insulation. The yellow spot is

[1] Crystal Barrel experiment - Helmholtz-Institut für Strahlen- und Kernphysik

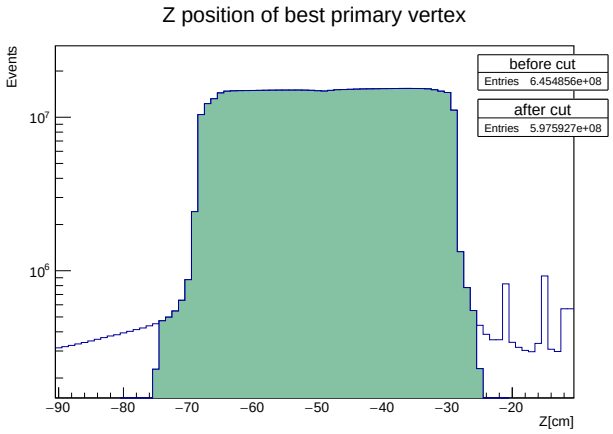

Figure 4.2: The green part are the events that remain after the cut.

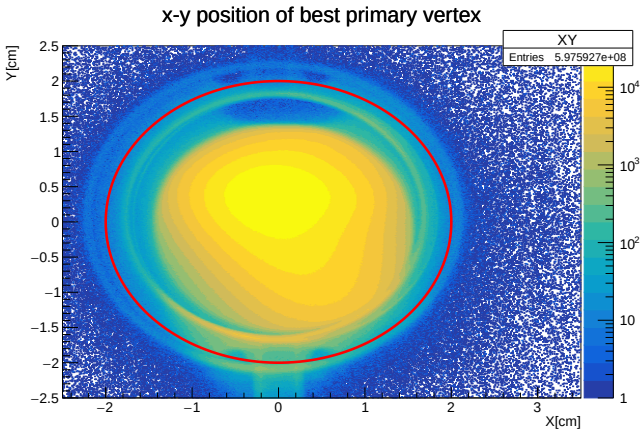

Figure 4.3: Events inside the red circle are the ones taken.

the beam shape. The blue spot at the coordinates (0,1.5) indicates, that the target was not completely filled.

4.2.2 Three charged particles

The final charged particles in the reaction are $\pi^+\pi^-\pi^-$, thus it is necessary to have three charged particles going out from the best primary vertex. The preselected data contains a small fraction of events with one outgoing track therefore the restriction for 3 outgoing tracks is important (Figure 4.4).

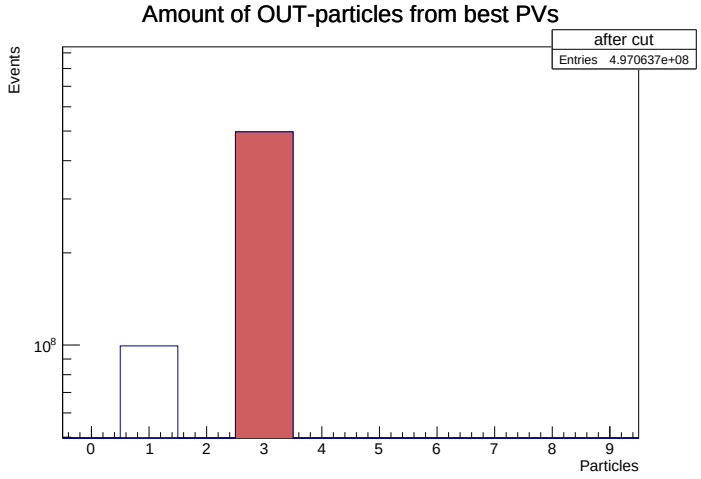

Figure 4.4: Required three charged particles leaving the best primary vertex

4.2.3 Charge conservation

For the reaction $\pi^- + p \to X + p$ the charge has to be conserved. The charge on the fermion side is maintained by the recoil proton. Therefore the charges of all remaining charged particles must add up to -1.

In PHAST there are two methods to get the charge of the particles, as can be seen in the 2D histogram 4.5. The first method extracts the charge from the bending of the track in the magnets. The second method uses a fit of the tracks that forces it to go through the best primary vertex, which might flip the sign of the charge. The mismatch of the two methods is only 0.01% of the total number of events. To guarantee reliable results, both methods are required to give -1.

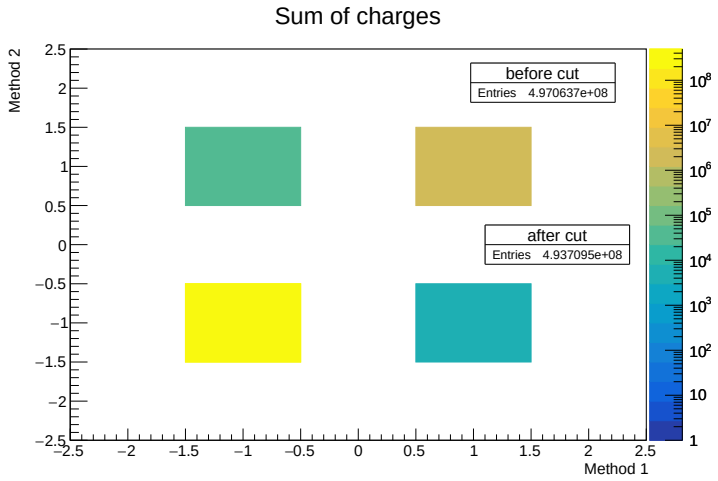

Figure 4.5: Charge conservation, comparison of the two methods described in the text

4.2.4 Calorimeters

The π^0 or η will decay electromagnetically to $\gamma\gamma$. Each γ will create a shower in the electromagnetic calorimeters (ECALs); some of the showers might overlap and therefore might be part of the same cluster. For this reason good clusters have to be selected, which are the ones with the following features:

- No track is associated with the cluster.
- A cut in time is set for the difference between cluster time and beam time: $-8\,\text{ns} \leq t_{\text{cluster}} - t_{\text{beam}} \leq 10\,\text{ns}$. Since a time calibration was performed, a peak is expected at $t = 0$ (Figure 4.6).
- Thresholds energies for ECAL1 $\geq 1\,\text{GeV}$ and ECAL2 $\geq 4\,\text{GeV}$ are chosen to decrease the noise that appears at low energies. Only the showers with the energy above those thresholds are considered for the further analysis. Compared to the Slot 3 production, the clustering algorithm was changed and a new calibration was performed [6].
- In Figure 4.7 we see a shadow of HCAL1 on ECAL2. This limits the effective area of ECAL2 to $-17{\cdot}3.83\,\text{cm} \leq y \leq 16{\cdot}3.83\,\text{cm}$, where the 3.83 cm is the side length of a cell. The reason is that a γ originating from the target will hit HCAL1 before it reaches ECAL2 and will start to shower. So the events collected in this part of the ECAL2 are not well defined particles.

The showers from both ECALs are collected and then only events with exactly two γ are saved (Figure 4.8).

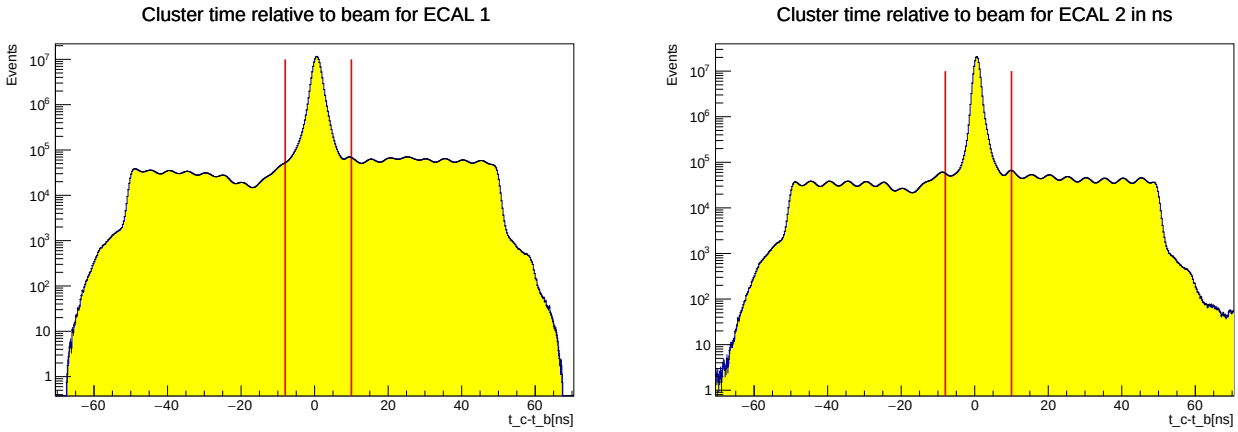

Figure 4.6: Time difference between beam and cluster for ECAL1 and ECAL2. The selection range is marked by the red lines.

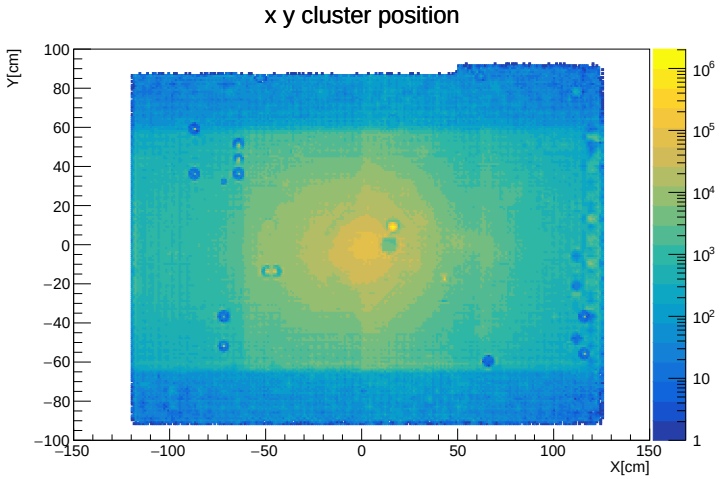

Figure 4.7: Cluster position on ECAL2, on the top and bottom part the "shadow" from the HCAL1 can be observed

4.2.5 Energy conservation

Energy must be conserved:

$$E_{beam} + E_{target} = E_X + E_{recoil}$$

First, we can make an approximation by neglecting the kinetic energy of the recoil proton, then the E_X is supposed to be equal to E_{beam}, thus the energy range is restricted to: 175 GeV $\leq E_X \leq$ 205 GeV

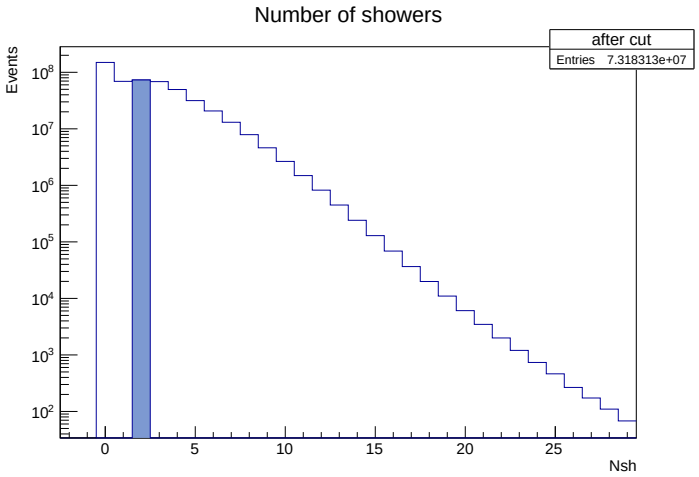

Figure 4.8: The showers obtained from both ECALs. In blue are the events with exactly two γ

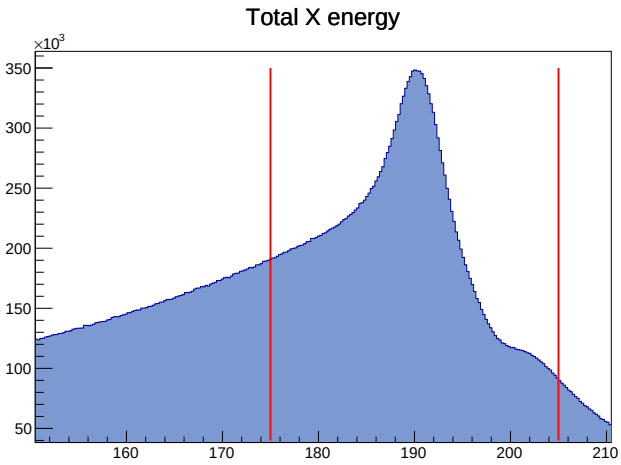

Figure 4.9: Energy of the X.

This concludes with the first stage of selection, that was carried out, following the steps, from the previous analysis for the Slot 3 production data ([10], [11]). The tables A.1 and A.2 show how the entry percentage changes after each selection.

Cut	Complete
Start	100 %
Trigger	79.2 %
Best primary ver	64.2 %
PV target	56.5 %
3 4 5 tracks	16 %
Charge sum	10.1 %
2 or 4 gammas	0.8 %
Energy cut	0.1 %

Table 4.1: Full statistics from first stage cuts on Slot 3 production.

Cut	Complete
After preselection	100 %
Trigger	94.3 %
Z pos	86.7 %
$r(x^2 + y^2)$	86.6 %
3 tracks	72.9 %
Charge sum	72.4 %
2 gammas	10.8 %
Energy cut	3.8 %

Table 4.2: Full statistics from first stage cuts on Slot 4 production.

4.3 Refined cuts

4.3.1 Target area

The cuts on the z position and r are more tight: $-67.5\,\mathrm{cm} < z < -29.5\,\mathrm{cm}$ and: $\mathrm{r} < 1.57\,\mathrm{cm}$. These cuts were not done on the first stage of selection in order to follow the steps from the previous analysis.

4.3.2 Beam energy recalculated

Since the energy of the beam is not measured it is known to be approximately 190 GeV. Using the kinematic constraint the precise value of the energy can be found.

The idea is to use momentum conservation and the energy of the outgoing particles:

Without knowing the momentum of the recoil proton and assuming the target is at rest, we get:

$$\begin{aligned} |p_{\vec{\mathrm{beam}}}| &= \sqrt{E_{\mathrm{beam}}^2 - m_{\mathrm{beam}}^2} \\ m_{\mathrm{target}} &= m_{\mathrm{recoil}} = m_{\mathrm{proton}} \\ |\vec{p}_{\mathrm{target}}| &= 0 \\ E_{\mathrm{recoil}} &= E_{\mathrm{beam}} + E_{\mathrm{target}} - E_X \end{aligned}$$

then the squared four-momentum transfer can be calculated:

$$\begin{aligned} t &= (p_{\mathrm{target}} - p_{\mathrm{recoil}})^2 = m_{\mathrm{target}}^2 + m_{\mathrm{recoil}}^2 - 2E_{\mathrm{recoil}}E_{\mathrm{target}} \\ &= 2m_{\mathrm{proton}}(m_{\mathrm{proton}} - E_{\mathrm{recoil}}) \\ &= 2m_{proton}(E_X - E_{beam}) \end{aligned} \tag{4.1}$$

Other way to obtain t is:

$$\begin{aligned} t &= (p_{\mathrm{beam}} - p_X)^2 \\ &= m_{\mathrm{beam}}^2 + m_X^2 - 2E_{\mathrm{beam}}E_X + 2|\vec{p}_X||\vec{p}_{\mathrm{beam}}|\cos\theta \end{aligned} \tag{4.2}$$

Where θ is the angle between the beam and the X. The next step is to set equation (4.1) equal to equation (4.2) and obtain E_{beam}.

After this the momentum can also be obtained by $|p_{\vec{beam}}| = \sqrt{E_{beam}^2 - m_{beam}^2}$, and a new Lorentz vector is formed.

4.3.3 Exclusivity cuts

To improve the results two final cuts are needed.

The cut on the outgoing energy revisited before is limited to the range:

$$186\,\text{GeV} \leq E_X \leq 196\,\text{GeV}$$

The second is the "coplanarity angle" $\Delta\phi$ which is the angle between the plane created by the X and the beam, and the plane created by the recoil proton and the beam:

$$\Delta\phi = \sphericalangle(\vec{p_X} \times \vec{p}_{\text{beam}}, \vec{p}_{RP} \times \vec{p}_{\text{beam}}) \tag{4.3}$$

To calculate it, it is used the momentum conservation to substitute $\vec{p}_{\text{beam}}$:

$$\vec{p_X} \times \vec{p}_{\text{beam}} = \vec{p_X} \times (\vec{p_X} + \vec{p}_{RP}) = \vec{p_X} \times \vec{p}_{RP} \tag{4.4}$$

$$\vec{p_{RP}} \times \vec{p}_{\text{beam}} = \vec{p}_{RP} \times (\vec{p_X} + \vec{p_X}) = \vec{p}_{RP} \times \vec{p_X} \tag{4.5}$$

Which means $\vec{p}_{RP} \times \vec{p}_{\text{beam}} = -\vec{p_X} \times \vec{p}_{\text{beam}}$, then the value expected is $\Delta\phi = \pm\pi$. The geometric angular resolution, caused by the individual RPD slabs influences the coplanarity [12]. From the y-axis of the Figure 4.10 the cut for the coplanarity can be seen.

$$\Delta\phi \geq 2.9 \tag{4.6}$$

The second cut is on the energy as on the first part:

$$186\,\text{GeV} \leq E_X \leq 196\,\text{GeV} \tag{4.7}$$

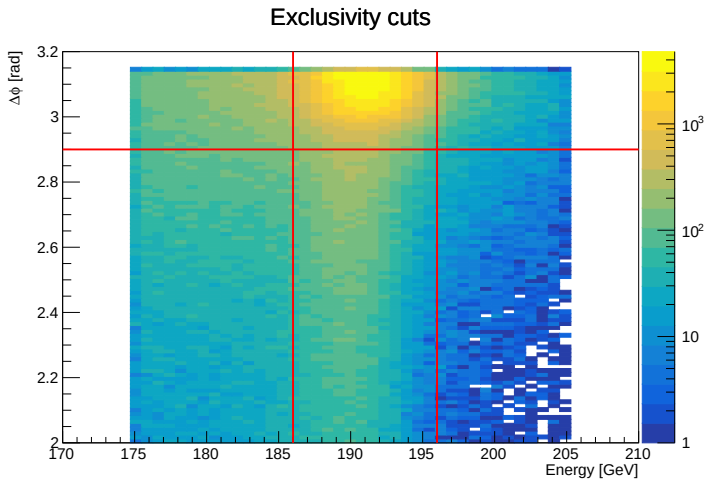

Figure 4.10: The exclusivity energy and $\Delta\phi$. The red lines show the cuts for each variable

4.3.4 π^0 or η

With the showers obtained in the first part of the selection (Figure 4.11), Lorentz vectors for the γs are constructed using the shower energy for the magnitude of the momentum, and the shower center together with the position of the vertex for the direction. And then the invariant mass of the $\gamma\gamma$ system can be calculated.

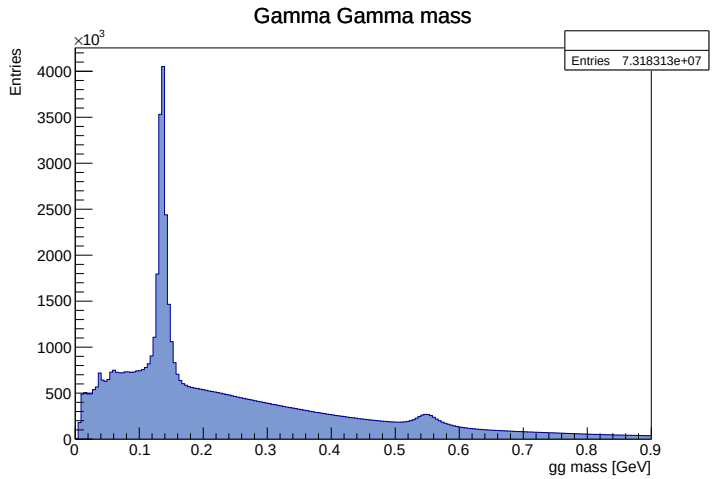

Figure 4.11: The mass of the 2 γ from the ECALs. The first peak corresponds to π^0 and the second one is the η.

- $|m(\gamma\gamma) - m_{\pi^0}| < 20\,\text{MeV}$ to get the π^0
- $|m(\gamma\gamma) - m_{\eta}| < 50\,\text{MeV}$ to get the η

CHAPTER 5

Results

5.1 $X^- \to \eta\pi^-$

First we use the π^0 obtained from the $\gamma\gamma$ combination (4.3.4), to determine the $(\pi^+\pi^-\pi^0)$ mass spectrum (Figure 5.1).

The structures seen in the invariant mass distribution 5.1 can be identified: Two peaks and a large background-like signal can be observed. The first peak is the η with a mass of 0.55 GeV and the peak next to it is the $\omega(782)$ with a mass of 0.78 GeV.

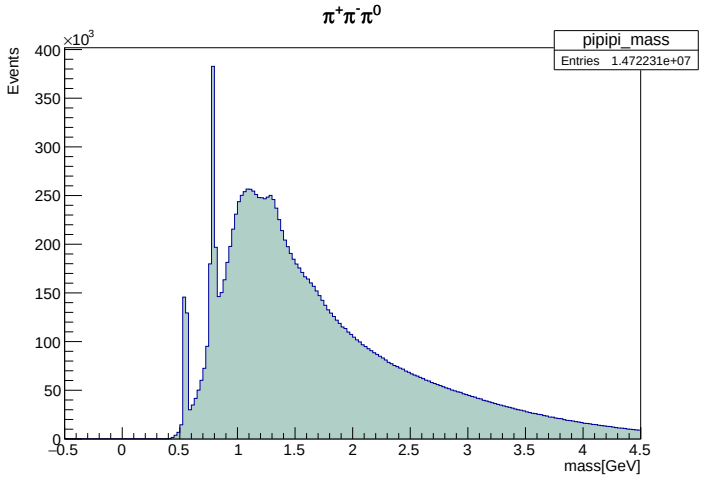

Figure 5.1: The $\pi^+\pi^-\pi^0$ mass spectrum. The η is around 0.55 GeV and next to it the $\omega(782)$ with a mass of 0.78 GeV

In order to identify the reaction we check the conservation of quantum numbers: the beam π^- has the quantum numbers $I^G = 1^-$, accordingly, the produced X^- also has $I^G = 1^-$.

Now the quantum numbers for the $\pi^+\pi^-\pi^0$ system give a G-parity $= -1$. It means that the G-parity is not conserved for the full reaction $X \to 4\pi$. But the $\eta \to \pi^+\pi^-\pi^0$ decay is G-parity violating, thus, the intermediate $\eta\pi^-$ state is allowed. On the other hand, for $\omega \to \pi^+\pi^-\pi^0$, G-parity is conserved, and with this $\omega\pi^-$ is forbidden. The reason why we still see the ω peak is that the real intermediate state is $\omega\pi^-\pi^0$, where the neutral pion is not seen by the detector.

After this a cut in mass is made to select only the η, needed for $\eta\pi^-$:

- $|m(\pi^+\pi^-\pi^0) - m_\eta| < 20\,\text{MeV}$

With the selected η candidates, we get the resulting final state of $\eta\pi^-$ (Figure 5.2), where the dominant peak is the $a_2(1320)$.

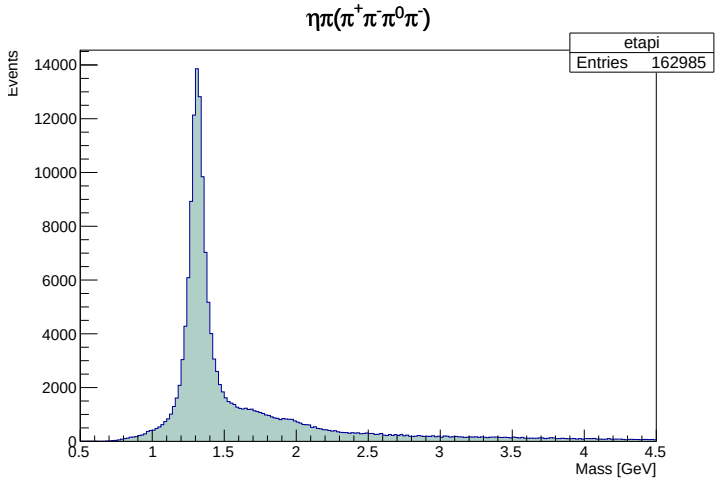

Figure 5.2: The $\eta\pi^-$ mass spectrum

5.2 $X^- \to \eta'\pi^-$

The η' is obtained from the $\pi^+\pi^-\eta$ spectrum.

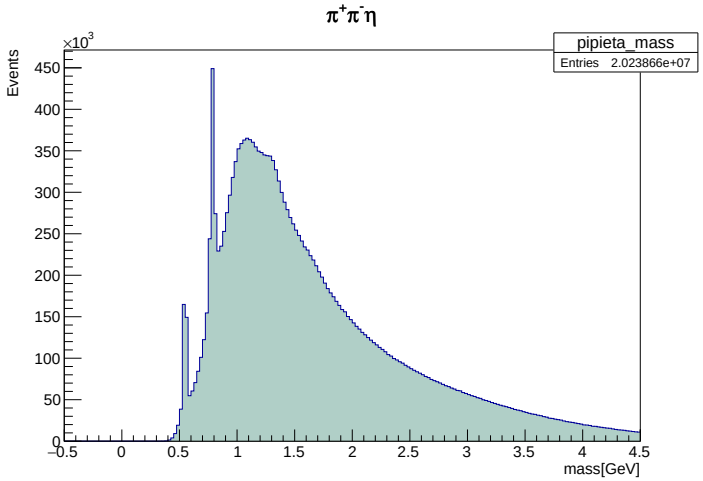

Figure 5.3: $\pi^+\pi^-\eta$ mass spectrum. The first peak is η' and the second can be either $\eta(1295)$ or $f_1(1285)$

In the plot 5.3, the first peak corresponds to the η^- and the second one can be either $\eta(1295)$ or $f_1(1285)$. Both particles are possible and in order to separate their contribution to the spectrum, a Partial Wave Analysis (PWA) is needed.

A cut in mass is made to select only the η', needed for the final state $X^- \to \eta'\pi^-$:

- $|m(\pi^+\pi^-\eta) - m_{\eta'}| < 50\,\text{MeV}$

After η' is obtained, the resulting final selection is $\eta'\pi^-$ (Figure 5.4), where again the $a_2(1320)$ is visible as a peak.

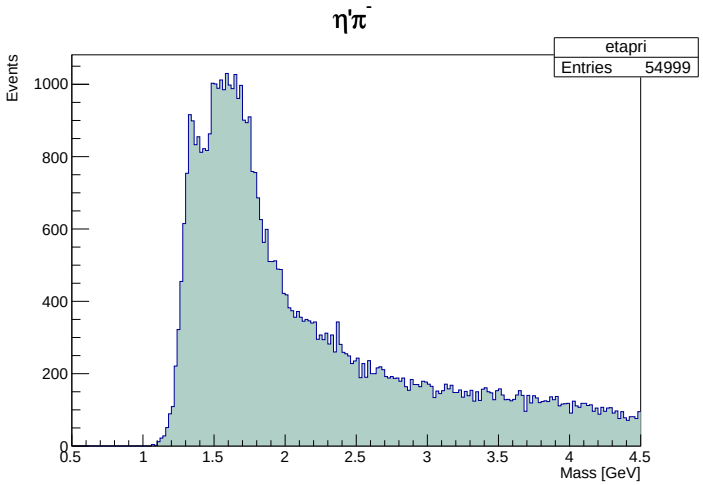

Figure 5.4: The $\eta\pi^-$ mass spectrum

5.3 Compare with Slot 3 production

After the final selection we can compare then the final number of events that remain. In this thesis no kinematic fit was performed after the π^0 selection. This fit could increase the number of events even further.

Entries	Slot 3	Slot 4	Ratio
$\eta\pi$	115754	162985	1.408
$\eta'\pi$	38954	54999	1.412

Table 5.1: Comparison of the number of events for $\eta\pi^-$ and $\eta'\pi^-$. We can see an increase for the number of events of $\sim 40\,\%$.

CHAPTER 6

Conclusions

The event selection for $\eta\pi$ and $\eta'\pi$ was performed, using the preselected data of the COMPASS experiment from 2008. The complete data sample of 3 TB was copied from the tapes at CERN and processed in Bonn.

As a starting point, similar cuts were applied to our data as in the previous analysis from 2012. Some of them had to be investigated further because, at first sight, the outcome differed from the expected results. One example the bin for RPD appeared to be empty while it is a requirement for DT0.

The number of events after the preselection was $7.1 \cdot 10^8$ and after all cuts 162985 and 54999 events remained for $\eta\pi$ and $\eta'\pi$, respectively.

In the $\pi^+\pi^-\pi^0$ spectrum we see two peaks at the masses of η and ω. The $\pi^+\pi^-\eta$ spectrum contained η', $\eta(1295)$ and $f_1(1285)$. In the final state $\eta\pi$ the peak for $a_2(1320)$ is visible. It also appears in $\eta'\pi$.

The next step in the study of the $\eta\pi^-$ and $\eta'\pi^-$ final states is a Partial Wave Analysis to separate the contributions of the different quantum numbers J^{PC}. In order to achieve this goal, one has to investigate the detector acceptance, including Monte Carlo simulations.

Bibliography

[1] C. Adolph et al.,
Odd and even partial waves of $\eta\pi^-$ and $\eta'\pi^-$ in $\pi^- p \to \eta^{(')}\pi^- p$ at 191 GeV/c,
Phys. Lett. B **740** (2015) 303, arXiv: 1408.4286 [hep-ex] (cit. on p. 1).

[2] C. Patrignani et al., *Review of Particle Physics*, Chin. Phys. **C40** (2016) (cit. on p. 5).

[3] P. Abbon et al., *The COMPASS Setup for Physics with Hadron Beams*,
Nucl. Instr. Meth. A **779** (2015) 69, arXiv: 1410.1797 [physics.ins-det]
(cit. on pp. 7, 8).

[4] P. Abbon et al., *The COMPASS Experiment at CERN*,
Nucl. Instr. Meth. A **577** (2007) 455, eprint: hep-ex/0703049 (cit. on p. 7).

[5] R. Panknin, *The Hadron Trigger 2008*, URL: https://twiki.cern.ch/twiki/pub/Compass/Trigger/HadronTrigger/panknin_hadron_trigger.pdf (cit. on p. 9).

[6] S. Uhl et al., *Diffractive Production of Final States decaying to $\pi^-\pi^0\pi^0$ and $\pi^-\eta\eta$*, 2013, URL: http://wwwcompass.cern.ch/compass/results/2013/february%5C_hadron%5C_2pi0%5C_2eta/suhl%5C_releasenote.pdf (cit. on pp. 13, 16).

[7] J. Barth, private communication, 2018 (cit. on p. 13).

[8] S. Wallner, *Event Preselection 2008*, URL: https://twiki.cern.ch/twiki/bin/view/Compass/HadronAnalysis/PreEventSelection2008 (cit. on p. 13).

[9] Y. Bedfer, *Vertex reconstruction*, URL: https://twiki.cern.ch/twiki/bin/view/Compass/DataReconstruction/CoralVertexing#PrimVertex (cit. on p. 14).

[10] T. Schlüter,
The $\pi^-\eta$ and $\pi^-\eta'$ Systems in Exclusive 190 GeV $\pi^- p$ Reactions at COMPASS (CERN),
PhD thesis: Ludwig-Maximilians-Universität München, 2012, URL: http://wwwcompass.cern.ch/compass/publications/theses/2012_phd_schlueter.pdf
(cit. on p. 18).

[11] C. Raab, *Analysis of the $\eta'\pi$ and $\eta\pi$ final states in COMPASS Data*, 2011, URL: http://wwwcompass.cern.ch/compass/publications/theses/2011_bac_raab.pdf
(cit. on pp. 18, 33).

[12] C. Dreisbach, *Study of elastic $\pi^- p$ scattering at COMPASS*,
MA thesis: Techn. Univ. München, 2014 (cit. on p. 21).

Appendix

APPENDIX A

Comparing results

This tables A.1 and A.2 show the results otained in 2012 ([11]) by the ones obtain now.

Cut	Sum	W33	W35	W37
Start	6013121609	1264032348	1907620614	2841468647
Trigger	4514085911	1000839072	1434392992	2078853847
Best primary ver	3827890956	810913642	1225881401	1791095913
PV target	3377377786	713660970	1078640544	1585076272
3 4 5 tracks	953331520	202024797	305753075	445553648
Charge sum	598861361	127622315	192356151	278882895
2 or 4 gammas	136350868	9899311	51616068	74835489
Energy cut	44896141	1062549	17895249	25938343

Table A.1: Full statistics from first stage cuts on Slot 3 production.

Cut	Sum	W33	W35	W37
After preselection	712264206	154394938	215773510	342095758
Trigger	645485538	145553838	195123057	304808643
Z pos	597592675	133882251	181085592	282624832
Radius	596409246	133661400	180754057	281993789
3 tracks	497063749	112551638	150683424	233828687
Charge sum	493709492	111849912	149640020	232219560
2 gammas	73183125	16635814	22129450	34417861
Energy cut	26208649	5836034	8049582	12323033

Table A.2: Full statistics from first stage cuts on Slot 4 production.

List of Figures

List of Tables